Published in final edited form as:

J Immunol. 2016 June 1; 196(11): 4713–4722. doi:10.4049/jimmunol.1502110.

The CD4 and CD3δε cytosolic juxtamembrane regions are proximal within a compact TCR-CD3-pMHC-CD4 macro-complex

Caleb R. Glassman[*], **Heather L. Parrish**[*], **Neha R. Deshpande**[*,+], and **Michael S. Kuhns**[*,+,‡]

[*]Department of Immunobiology, The University of Arizona College of Medicine, Tucson, AZ 85724, USA

[+]The Arizona Center on Aging, The University of Arizona College of Medicine, Tucson, AZ 85724, USA

[‡]The BIO-5 Institute, The University of Arizona College of Medicine, Tucson, AZ 85724, USA

Abstract

T-cell receptors (TCRs) relay information about peptides embedded within major histocompatibility complex molecules (pMHC) to the immunoreceptor tyrosine-based activation motifs (ITAMs) of the associated CD3γε, CD3δε, and CD3ζζ signaling modules. CD4 then recruits the Src kinase, Lck, to the TCR-CD3 complex to phosphorylate the ITAMs, initiate intracellular signaling, and drive $CD4^+$ T-cell fate decisions. While the six ITAMs of CD3ζζ are key determinants of T cell development, activation, and the execution of effector functions, multiple models predict that CD4 recruits Lck proximal to the four ITAMs of the CD3 heterodimers. We tested these models by placing FRET probes at the cytosolic juxtamembrane regions of CD4 and the CD3 subunits to evaluate their relationship upon pMHC engagement in mouse cell lines. The data are consistent with a compact assembly in which CD4 is proximal to CD3δε, CD3ζζ resides behind the TCR, and CD3γε is offset from CD3δε. These results advance our understanding of the architecture of the TCR-CD3-pMHC-CD4 macro-complex and point to regions of high CD4-Lck-ITAM concentrations therein. The findings thus have implications for TCR signaling, as phosphorylation of the CD3 ITAMs by CD4-associated Lck is important for $CD4^+$ T-cell fate decisions.

Introduction

Individual peptides embedded within class II major histocompatibility complex molecules (pMHC) create composite surfaces that encode essential information for T-cell-mediated immunity. Thymocytes and $CD4^+$ T-cells survey the libraries of pMHC expressed on thymic epithelial cells (TECs) or antigen presenting cells (APCs), respectively, with clonotypic T-cell receptors (TCRs) that relay mechanical information about TCR-pMHC interactions across the membrane to the immune receptor tyrosine-based activation motifs (ITAMs) of the associated CD3 signaling modules (CD3δε, CD3γε, and CD3ζζ) (1–5). This information is then converted to chemical signals when CD4, which also binds class II MHC, recruits the Src kinase $p56^{Lck}$ (Lck) to the TCR-CD3 complex to phosphorylate the ITAMs (6, 7). In this

Address correspondence to Dr. Michael S. Kuhns. Phone: (520) 626-6461, Fax: (520) 626-2100, ; Email: mkuhns@u.arizona.edu.

way, pMHC engagement by both TCR and CD4 acts as a coincidence detector to drive the generation, maintenance, and function of a pMHC-specific TCR repertoire. There are ten ITAMs within a TCR-CD3 complex, with CD3δ, γ and ε having one each and CD3ζ having three. The quantity and quality of ITAM phosphorylation determines cell fate decisions, with fewer than seven functional ITAMs per complex leading to a breakdown in central tolerance (8, 9). Thus, assembly of a TCR-CD3-pMHC-CD4 macro-complex is key to $CD4^+$ T-cell development and effector functions.

The sensitivity and specificity of this macro-molecular machinery have inspired considerable interest in how it works. Although TCR-CD3 crosslinking with monoclonal antibodies (mAbs) can activate T-cells, not all mAbs can induce this outcome (10); furthermore, not all TCR-pMHC interactions of seemingly sufficient affinity activate T-cells if they dock in a noncanonical topology (11). Thus, an ordered relationship of signaling molecules appears to be important for T-cell activation, particularly when receptors are confronted with their natural ligands (1, 2, 12, 13).

In support of this idea, two crystallography studies indicate that a V-like arch is formed when CD4 and the TCR simultaneously bind a pMHC. One structure included the D1 and D2 domains of CD4 in complex with MHC but without a TCR, while the other constituted a ternary complex of a TCR, pMHC, and the four extracellular domains of a CD4 molecule that was affinity maturated for binding to MHC (14, 15). Both structures suggest that the TCR-pMHC axis constitutes one arm of the arch while CD4 constitutes the other and the CD4-MHC binding site forms the apex.

Since TCR-pMHC interactions occur via a canonical docking orientation, the implication is that a geometrically constrained TCR-CD3-CD4-pMHC architecture is functionally mandated to achieve a specific relationship between Lck and the ITAMs for proper signaling. Mutagenesis and NMR data place the ectodomains of CD3δε and CD3γε on one side of the TCR, with CD3δε and CD3γε positioned inside the arch formed with CD4, while EM data indicate that these heterodimers are nested near the base of the TCR (1, 16–20). Due to the turn of the TCRα transmembrane helix and ~140° offset of the positively charged residues that interact with CD3ζζ and CD3δε, CD3ζζ should reside on the opposite side of the TCRα subunit from CD3δε (21). Also, because the CD3 heterodimers have short, rigid connecting peptides and the existing structural data for activating immune receptor transmembrane domains (TMDs) indicate a minimal crossing angle, the CD3 TMDs are likely to emerge into the cytoplasm in a spatial orientation that roughly mimics their ectodomain (22, 23). Consequently, Lck is predicted to be closest to the four ITAMs of the CD3 heterodimers upon pMHC engagement (1, 2, 12, 16). *A priori*, such a model is surprising since the six ITAMs within the CD3ζζ signaling module (three per subunit) clearly play an important role in T-cell development and activation (6, 8, 9). Testing this model is thus necessary to gain better insights into the architecture and function of the TCR-CD3-pMHC-CD4 macro-complex.

Here we used Förster Resonance Energy Transfer (FRET) to experimentally assess the spatial relationship between the cytoplasmic juxtamembrane (JM) regions of CD4 and the CD3γ, δ, ε, and ζ subunits upon concurrent CD4 and TCR engagement of agonist pMHC.

Replacing the intracellular domains with FRET probes ensured that any proximity measurements were dependent upon binding of CD4 and the TCR to pMHC, but independent of signaling or post-signaling interactions that may tether CD4 to the TCR-CD3 complex (7). Such a system allowed us to make predictions about the native spatial relationships between kinase and substrate in the context of a living cell. The data indicate that CD4 adopts an ordered spatial arrangement with respect to the TCR-CD3 complex only when both the TCR and CD4 bind an agonist pMHC. Therein, the JM region of CD4 is positioned closer to that of CD3δ than CD3γ and closer to the CD3ε subunits than the CD3ζζ subunits. The implications of these data for the architecture of the TCR-CD3-pMHC-CD4 macro-complex, and its function in early signaling events, are discussed.

Materials and Methods

Cell lines and Constructs

M12 and 58$\alpha^{-}\beta^{-}$ T-cell hybridoma lines were generated by retroviral transduction and drug selection, as previously described (3, 24–26). The 5c.c7 TCR, which is specific for the moth cytochrome c peptide (MCC 88–103) in I-E^{K} (27, 28), was used in this study in complex with C-terminally truncated CD3ε (aa:1–139), δ (aa:1–132), γ (aa:1–143) and ζ (aa:1–57) subunits (CD3xT) or full length CD3 subunits where indicated in the text (3, 17). When a CD3T subunit was expressed as a fusion with monomeric enhanced GFP (mEGFP), we used a GGGSAAAG linker. C-terminally truncated versions of CD4 (CD4T: aa1–421), with or without the Δbind mutation (aa:68–73 KGVLIR to DGDSDS), fused to mCherry via a AAAG linker were used in this study (26, 29). Glycine-based linkers were used for our fusion proteins because flexibility is required to allow equivalent probability of dipole alignment between FRET pairs, and even a single glycine in a dipeptide linker can allow a strand to double back upon itself (30–34). The AAA segment of each linker represents the reading frame of a NotI restriction enzyme cut site used for cloning. This was chosen because Ala has been used with Gly in flexible linkers (35). Furthermore, poly-Ala peptides have been reported to assume similar backbone conformation diversity to poly-Gly (36) provided the AAA stretch is not flanked by Glu and Lys residues, which it was not in our study (37). Cell lines were assessed for TCR-CD3 and CD4 surface expression by flow cytometry.

MSCV-based retroviral expression vectors pP2 (IRES-puromycin resistance) and pZ4 (IRES-zeocin resistance) were used for the generation of mouse cell lines (16). We took advantage of the 2A cleavage system to generate poly-cistronic constructs that reduced the number of constructs needed per cell line (8).

Experimental M12 FRET lines were generated using constructs encoding CD3ε$T^{(G)}$-T2A-5c.c7α, CD3ζ$T^{(G)}$-T2A-5c.c7β, and CD3δ$T^{(G)}$-T2A-CD3γ$T^{(G)}$ along with a construct encoding CD4T^{mCh} or CD4$T^{\Delta bind.mCh}$. The CD3x$T^{(G)}$ indicates that constructs were built encoding only the truncated CD3 subunit, or a fusion of a truncated CD3 subunit to mEGFP (G) to generate cell lines expressing a single CD3-mEGFP species. For cell lines without a CD3ζ-mEGFP fusion, CD3ζ was fused to the biotin acceptor peptide, AP-3. This is a short tag that was considered irrelevant for these studies, but is connected by the same linker as mEGFP. M12 control lines consisted of C-terminally truncated CD28 (CD28T aa:1–179) or

PD-1 (PD-1T aa:1–199) fused to mEGFP and mCherry via an AAAG linker and were co-transduced with 2.5 equivalents of full-length CD3 subunits lacking CD3ζ to account for viral load.

To generate CD3εT^{G}::CD4T^{mCh} or CD3ζT^{G}::CD4T^{mCh} 58α^{-}β^{-} cell lines for FRET comparisons, parental cells were transduced with vectors encoding CD3εT^{G}-T2A-5c.c7α and CD3ζT-T2A-5c.c7β, or CD3εT-T2A-5c.c7α and CD3ζT^{G}-T2A-5c.c7β along with a CD4 constructs and a construct encoding all full-length versions of the CD3 subunits (8, 16). To generate 58α^{-}β^{-} cell lines comparing CD3δT^{G}::CD4T^{mCh} and CD3γT^{G}::CD4T^{mCh} FRET, cells were transduced with individual constructs encoding 5c.c7α, 5c.c7β, CD3xT-mEGFP, CD4TmCherry, and all full-length CD3 subunits.

58α^{-}β^{-} control cell lines were transduced with individual constructs encoding 5c.c7α, 5c.c7β, PD-1T (aa:1–199) fused to mEGFP and mCherry via an AAAG linker and all full-length CD3 subunits. Further information is available upon request.

Soluble proteins for bilayers and immobile surfaces

Production of soluble pMHC and ICAM-1 was performed with a baculovirus expression as described elsewhere (3, 26).

Lipid bilayers

Bilayers were prepared with a lipid mixture consisting of 97.5 mol % POPC, 1 mol % DGS NiNTA, 1 mol % biotin-CAP PE and 0.5 mol % DOPE-PEG5000 were extruded to generate unilaminar vesicles (Avanti Polar Lipids) (26, 38). Liposomes were injected onto a cleaned glass coverslip and bilayer mobility was assed by photoablation recovery of streptavidin conjugated to APC as previously described (26, 38). For TCR engagement experiments, each well received 0.05μg of MCC:I-E^{K} and 0.08μg ICAM-1 to produce an agonist pMHC density of approximately 60mol/micron^{2} (17, 26, 38).

Peptide-MHC Surfaces

Biotinylated poly-L-lysine coated coverslips were incubated with 5μg/ml streptavidin, washed, and incubated with 400μl PBS+2%BSA+0.01% Sodium Azide containing a total pMHC-biotin concentration of 5μg/ml (Hb:I-E^{k} and MCC:I-E^{k}) and 0.5μg/ml biotinylated anti-H2-D^{d} (3, 39).

Microscopy

TIRFM was performed at 37°C, 5% CO_2, and 50% relative humidity. Cells were adhered to the glass coverslip, lipid bilayers or immobile surface for 20 minutes and then imaged for 20–30 minutes following adhesion. TIRF images were acquired using a Marianas workstation built on a Zeiss Axio Observer Z1 (Intelligent imaging innovations (3I)) with a Zeiss fluorescent microscope using a 63× Zeiss TIRF objective coupled to a Zeiss motorized TIRF slider (NA 1.46). TIRFM was performed with a Laser Stack (3I) containing 50mW 488nm and 561nm solid-state lasers set at 20% power output. Photoablation of mCherry was performed with a Vector high-speed point scanner (3I) at 100% 561nm laser output within a

6.45 μm^2 region of interest (ROI). Images were collected at 500 millisecond intervals (Photometrics Evolve EMCCD; 1 pixel = 0.25μm (H) × 0.25μm (V) at 63×).

Image Analysis

Median mEGFP and mCherry intensity for the region of interest targeted for mCherry ablation were background subtracted using SlideBook6 (3I) and exported. Data were processed in MATLAB (MathWorks) and FRET was calculated as $FRET_E = 1- (Q/DQ)$ where Q (quenched) is the mEGFP intensity prior to mCherry ablation and DQ (dequenched) is the mEGFP intensity following ablation as previously reported (3, 26). Efficiency of mCherry ablation was calculated as the ratio of post to prebleach mCherry intensity, Abl=mCh(postbleach)/mCh(prebleach). Subsets designated ‘All cells’ in the figures had mCherry ablation below 12.5% prebleach intensity as described previously (3, 26). This resulted in the analysis of populations with an average ablation below 10% prebleach intensity (not shown). Subsets designated ‘Matched subset’ included events with ablation below 12.5% of prebleach mCherry intensity in which analyzed populations were matched for mCherry intensity prior to photobleaching and GFP intensity following photobleaching to account for differential donor quenching in experimental conditions as well as GFP/mCherry ratio.

FFLISA

1% n-Dodecyl-b-D-maltoside (DDM) lysates from CD3xT^G cell lines were subject to immunoprecipitation with 6.0μm polystyrene beads (Polysciences) coated with anti-TCRβ mAbs (H57–597 Biolegend). After washing, the beads were then probed with anti-TCRα (α–Vα11 RR8-1 APC eBioscience) and anti-CD3ε (145–2C11 PE BD) with fluorescently labeled mAbs. Analysis was then performed by flow cytometry to assess co-precipitation of TCRα, CD3ε, and CD3xT^G (mEGFP) with TCRβ similarly to previously described protocols (29, 40, 41).

Statistical Analysis

All statistical analyses were performed with Prism 6 (GraphPad Software, Inc). As the data presented here are non-parametric, Mann-Whitney test and Kruskal-Wallis test with Dunn’s multiple comparisons were used where appropriate.

Results

Proximal association of CD4 and CD3δ upon TCR and CD4 engagement of agonist pMHC

The existing experimental data suggest that the formation of a TCR-CD3-pMHC-CD4 macro-complex positions Lck closest to the ITAMs of CD3δε (42). Consequently, we transduced B cell lymphoma M12 cells, which do not express endogenous TCR-CD3 subunits, to express the 5c.c7 TCR, C-terminally truncated CD3γ, ε, and ζ subunits (CD3γT, εT, and ζT) that lack ITAMs and cannot signal (3, 24), and CD3δT fused to mEGFP (CD3δT^G) as the FRET donor. We also expressed C-terminally truncated CD4 (CD4T) fused at the JM region to mCherry (CD4T^{mCh}) as a FRET acceptor. FRET was measured by donor recovery after acceptor photobleaching via total internal reflection fluorescence microscopy (TIRFM) to determine a relative FRET efficiency value ($FRET_E$) for molecules on the cell

membrane, as previously described (3, 26). This experimental approach allowed us to reduce the question to one of spatial proximity driven purely by pMHC engagement via the TCR and CD4 in the absence of competition with endogenous subunits, signaling, and signaling feedback.

CD3δT^{G}::CD4T^{mCh} FRET$_{E}$ was first measured for M12 cells adhered to glass coverslips in order to establish a baseline signal in the absence of pMHC engagement. Coverslips coated with immobile agonist pMHC were then used to determine if concurrent TCR and CD4 engagement of agonist pMHC increased FRET between CD3δ and CD4 (Figure 1A) (26). Since we have previously established that disulfide-bonded CD28 homodimers and PD-1 monomers serve as positive and negative controls, respectively, for FRET in M12 cells we analyzed CD3δT^{G}::CD4T^{mCh} FRET$_{E}$ along with these controls (3, 26). No difference in FRET$_{E}$ was observed between the PD-1T^{G}::PD-1T^{mCh} negative control and our experimental CD3δT^{G}::CD4T^{mCh} cells imaged on glass coverslips. This is consistent with data suggesting that CD4 and TCR do not pre-associate in an unengaged state (43). Adherence of CD3δT^{G}::CD4T^{mCh} cells to glass coverslips functionalized with agonist pMHC resulted in a significant increase in CD3δT^{G}::CD4T^{mCh} FRET$_{E}$ compared to cells on uncoated coverslips or the negative control cells, indicating that concurrent TCR and CD4 engagement of agonist pMHC positions CD3δ and CD4 in a close spatial relationship (Figure 1B).

While the CD3δT^{G}::CD4T^{mCh} FRET$_{E}$ signal was lower than that of the positive control cells, it is unclear if this is due to differences in distance between FRET donor and acceptor, the frequency of productive FRET pairs, or both. In the case of CD3δ::CD4 FRET, coordinate binding of CD4 and TCR to an agonist pMHC creates a transient mEGFP and mCherry pairing for a subset of TCR and CD4 molecules that engage pMHC on an immobile surface. This is because CD4 and the TCR have been shown by super resolution imaging to inhabit distinct membrane domains (43). Consequently, the number of TCRs within a membrane domain that are available to engage the same pMHC as a CD4 molecules in a distinct membrane domain appears to be physically limited to those that are located at the boundary of each membrane domain (43). In contrast, disulfide-bonded CD28 homodimers will speciate into CD28T^{G}::CD28T^{mCh}, CD28T^{G}::CD28T^{G}, and CD28T^{mCh}::CD28T^{mCh} pairs within the same membrane domain based on the relative expression of FRET constructs. These distinctions are important because FRET$_{E}$ measurements are based on changes in the fluorescent intensity of all FRET donors within a region of interest after acceptor ablation of all donor molecules, whether or not they are paired with an acceptor. Due to the complications outlined above, and differences in expression profiles, comparisons between the CD3δT^{G}::CD4T^{mCh} FRET$_{E}$ and CD28 provide limited quantitative information.

Given the challenges associated with comparing FRET between distinct molecular species we also approached the problem by asking if mutating the D1 domain region of CD4, which binds class II MHC in crystal structures (14, 15), would impair the CD3δT^{G}::CD4T^{mCh} FRET$_{E}$ signal observed on pMHC-coated coverslips. To this end, we used a CD4T$^{\Delta bind}$ mutant that impairs T-cell hybridoma activation (26, 29). Here, CD3δT^{G}::CD4T$^{\Delta bind.mCh}$ FRET$_{E}$ was significant lower than CD3δT^{G}::CD4T^{mCh} FRET$_{E}$ at the bulk population level

(Figure 1C). One caveat to this approach is that CD4-MHC interactions influenced accumulation of CD4 at the contact interface (Figure 1D–F). But, this difference in donor and acceptor concentrations is unlikely to be responsible for the difference in FRET efficiency as intensity and ratio matched subsets showed a similar reduction in $FRET_E$ for the $CD3\delta T^G$::$CD4T^{\Delta bind.mCh}$ compared to the $FRET_E$ measured in $CD3\delta T^G$::$CD4T^{mCh}$ cells (Figure 1D–G). No difference was observed between the two cell lines on glass coverslips (Figure 1H), again demonstrating pMHC-dependence for the observed FRET. Altogether, these data strongly suggest that the $CD3\delta T^G$::$CD4T^{mCh}$ FRET results from concurrent TCR and CD4 engagement.

We next used mobile lipid bilayers presenting MCC:I-E^k and ICAM-1 to assess if these differences in FRET would be observed between the $CD3\delta T^G$::$CD4T^{\Delta bind.mCh}$ and $CD3\delta T^G$::$CD4T^{mCh}$ $FRET_E$ cells under more physiological conditions (Figure 2A). Again, we saw a decrease in FRET efficiency with the Δbind mutation, consistent with the results obtained on immobile surfaces (Figure 2B).

Taken together, the data suggest that the CD4 and CD3δ JM regions assume a close spatial proximity that depends upon the D1 domain of CD4 binding class II MHC, but does not require signaling. However, since TCR-CD3 complexes and CD4 accumulate at the binding interface, these data alone do not demonstrate an ordered spatial relationship. The observed $CD\delta T^G$::$CD4T^{mCh}$ FRET could be explained by random FRET interactions occurring in trans due to increased molecular concentrations (i.e. clustering) rather than a defined orientation enforced by specific interactions.

Coordinate TCR-pMHC and CD4-MHC interactions create an ordered CD4-CD3 spatial relationship

If $CD3\delta T^G$::$CD4T^{mCh}$ FRET results from random clustering then at any given point CD4 should, on average, be equidistant to all CD3 subunits. Alternatively, if FRET is occurring as a consequence of the formation of an ordered structure, then differences in $FRET_E$ should be observed between CD4 and the CD3 subunits based on the relative distances of their defined spatial relationships. To test these possibilities, we generated M12 cells expressing $CD4T^{mCh}$ and TCR-CD3 complexes containing $CD3\delta T^G$, $CD3\gamma T^G$, $CD3\varepsilon T^G$, or $CD3\zeta T^G$. Each CD3 subunit was fused to mEGFP via a common flexible linker (GGGSAAAG) that should allow the probe to extend beyond the short ICDs of the TCR (~5–9aa) and other truncated CD3 subunits (~5aa) and allow for an equivalent probability of dipole alignment. Because the CD3 intracellular domains, which do not play a role in complex assembly (3, 16, 17, 21), are largely absent in this system they should not inadvertently impact the rotation or position of the CD3-associated mEGFP. This design strategy should make FRET a function of the spatial position of the donor within the TCR-CD3 complex relative to the position of a CD4-associated acceptor when both the TCR and CD4 engage a pMHC. Consequently, any differences in $FRET_E$ between compared lines should reflect the distance of the particular CD3 JM regions relative to CD4 if an ordered macro-complex is formed. In our experiments, $CD3\delta T^G$ and $CD3\gamma T^G$ were compared directly since each is present only once in a single TCR-CD3 complex, and $CD3\varepsilon T^G$ and $CD3\zeta T^G$ were compared directly since there are two copies per complex.

Cell surface expression of TCR-CD3 complexes was confirmed by flow cytometry (not shown) as well as by TIRFM (Figure 3). Since the TCR only traffics to the cell surface in association with the CD3 subunits, these data strongly suggest that the FRET probes do not negatively impact complex assembly. To further confirm that fusing mEGFP to the individual CD3 subunits did not differentially impact complex assembly, we assessed the composition of the TCR-CD3 complexes using a flow-based flourophore-linked immunosorbant assay (FFLISA). Appropriate complex assembly involves the incorporation of two CD3ε per TCR-CD3 complex, independent of the mEGFP tagged CD3 subunit, whereas mEGFP will be present according to the copy number of the tagged subunit: one for CD3δ and CD3γ, or two for CD3ε and CD3ζ. Comparison of anti-CD3ε intensities with mEGFP levels revealed proportional signal (i.e. diagonal) for the CD3δT^G versus CD3γT^G and CD3εT^G versus CD3ζT^G cell lines, with CD3εT^G and CD3ζT^G shifted towards brighter mEGFP signal (Supplement 1A). This was confirmed by analysis of beads with matched TCRα intensities (i.e. equivalent αβTCR load). In matched samples, the ratio of mEGFP signal relative to CD3ε staining was similar between the CD3δT^G and CD3γT^G lines and between the CD3εT^G and CD3ζT^G lines (Supplement 1B). The slightly lower ratio of CD3ζT^G compared with CD3εT^G is expected due to the presence of partially assembled complexes, since it is well established that CD3ζ is the last subunit to join the complex and partially assembled complexes lacking CD3ζ can be found in whole cell lysates (21, 44). These data establish that the mEGFP probes do not differentially impact complex assembly.

Significantly higher $FRET_E$ was measured for CD3δT^G::CD4T^{mCh} than CD3γT^G::CD4T^{mCh} for ratio and intensity matched subsets on bilayers (Figure 3A). Likewise, CD3εT^G::CD4T^{mCh} was significantly higher than CD3ζT^G::CD4T^{mCh} for ratio and intensity matched subsets on bilayers (Figure 3B). These data are best explained by the formation of an ordered macro-complex upon coordinate TCR and CD4 binding to pMHC. Of note, no difference in $FRET_E$ was observed on glass coverslips for the relevant comparisons (Figure 3C–D).

We next asked if FRET between the distal CD3γ and CD3ζ subunits was dependent on CD4 engagement of MHC. Analysis of matched subsets revealed that the FRET efficiencies of CD3γT^G::CD4T^{mCh} and CD3ζT^G::CD4T^{mCh} were greater than their CD4$T^{\Delta bind.mCh}$ counterparts (Figure 3E–F). These data indicate that the observed FRET was dependent on CD4 engagement.

As a second approach for resolving random versus ordered FRET between CD4 and the TCR-CD3 complex, we measured FRET on immobile surfaces coated with agonist pMHC diluted into non-stimulatory pMHC. These surfaces prevent the cells from gathering agonist pMHC into a high local concentration, so at low agonist concentrations any measured FRET should be as a consequence of concurrent TCR-CD3 and CD4 association with an agonist ligand surrounded by null ligands. Indeed, our streptavidin capture system allows for the possibility of pMHC molecules being presented in orientations that are not accessible to TCR, CD4, or both, further reducing the actual availability of agonist pMHC for coordinate TCR and CD4 engagement. Since our cells express the 5c.c7 TCR that recognizes the moth cytochrome c peptide (88–103) presented in I-E^k (MCC:I-E^k) as an agonist pMHC, we diluted MCC:I-E^k into a null pMHC complex comprising the mouse hemoglobin d allele

peptide (64–76) presented in I-E^k (HB:I-E^k). This null ligand has previously been shown to lack co-agonist activity for the 5c.c7 TCR (45).

Analysis of $FRET_E$ for a titration of agonist into null pMHC revealed dose-dependent FRET. CD3δT^G::CD4T^{mCh} $FRET_E$ was observed to be higher than CD3γT^G::CD4T^{mCh} $FRET_E$, while CD3εT^G::CD4T^{mCh} $FRET_E$ was higher than CD3ζT^G::CD4T^{mCh} $FRET_E$ across the titration range (Figure 4A–B), including at low ligand densities (Figure 4C–D). Collectively, these data are best explained by non-random FRET between CD4 and the TCR-CD3 complex upon coordinate TCR and CD4 binding of agonist pMHC.

The same spatial relationship occurs in T-cell membranes

Finally, we measured $FRET_E$ between CD4 and each CD3 subunit in 58α$^-$β$^-$ T-cell hybridomas to verify that the spatial proximity of these molecules demonstrated the same hierarchy when measured in a T-cell membrane environment in the presence of full-length, signaling-competent CD3 subunits (26). First, we compared CD3δT^G::CD4T^{mCh} $FRET_E$ on lipid bilayers to negative control 58α$^-$β$^-$ (PD-1T^G::PD-1T^{mCh}) cells that expressed TCR-CD3 complexes and were able to adhere to the bilayers (Figure 5A). CD3δT^G::CD4T^{mCh} $FRET_E$ was observed to be higher than the negative control (Figure 5B). This signal was dependent on CD4 binding to MHC as the CD4$T^{\Delta bind}$ mutant reduced this signal (Figure 5C–D). Importantly, CD3δT^G::CD4T^{mCh} $FRET_E$ was higher than CD3γT^G::CD4T^{mCh} $FRET_E$, and CD3εT^G::CD4T^{mCh} $FRET_E$ was higher than CD3ζT^G::CD4T^{mCh} $FRET_E$ (Figure 5E–F). The magnitude of these differences are smaller than those observed in the M12 system. This is likely due to the presence of untagged subunits or the potential for signaling and signaling feedback. Altogether, these data indicate that the spatial relationships observed in M12 cells in the absence of CD3 ITAMs holds in T-cell hybridomas expressing a full complement of ITAMs.

Discussion

Here we show that CD4 adopts an ordered spatial relationship with the TCR-CD3 complex when the TCR and CD4 bind to agonist pMHC. The results are important for our understanding of the architecture of this macro-complex, and provide a conceptual framework for further interrogating its function.

Overall, the data shed light on the subunit arrangement within the TCR-CD3-pMHC-CD4 macro-complex. Specifically, they indicate that CD4 JM region resides closer to the JM region of CD3δ than to CD3γ and closer to the JM region of the CD3 heterodimers than to CD3ζζ. TCRα is known to interact with CD3δε and CD3ζζ via positively charged residues that are offset by ~140° in its transmembrane domain (21). This suggests that the CD3ζζ JM regions are similarly displaced (i.e. ~140°) relative to the JM regions of CD3δε when associated with TCRα (23). Within this context, the simplest interpretation of our data is that the JM regions of CD3δε are between the JM regions of CD4 and TCRα, with the CD3ζζ JM regions sitting behind TCRα. Since CD3γε interacts via transmembrane charge interactions with TCRβ, its JM regions would be offset at a distance from CD3δε (21).

Three distinct arrangements of the TCR-CD3 complex subunits have been proposed and are considered here within the TCR-CD3-pMHC-CD4 macro-complex. Our FRET data are inconsistent with a model in which CD3γε is positioned in line with CD4 such that CD3δε is situated adjacent to CD3γε, but offset at a greater distance from CD4 (12). Slight adjustments in the placement of the CD3 heterodimers might reconcile these differences for this model; however, previous proximity analysis of the CD3 JM regions does not support a juxtaposed placement of CD3δ and CD3γ (17). Furthermore, due to the 140° offset of the TCRα transmembrane domain charge residues that interact with CD3δε and CD3ζζ, too much adjustment would place CD4 closer to CD3ζζ than either CD3ε. The data presented here are compatible with models in which CD3δε and CD3γε are either situated on opposite sides of the TCR (22, 46), or reside on one side of the TCR such that the subunits are ordered δ:ε:ε:γ (1, 2, 16, 17). This last model is most consistent with other experimental data, as well as recent NMR data, so we currently consider it the best approximation of the subunit organization of the TCR-CD3 complex (1, 19).

When integrating this model with the ternary arched crystal structure of TCR-pMHC-CD4 (Supplement 2) what is most striking is that, by the general approximations allowed by such modeling, the JM regions of CD3γ and either CD3ζζ subunit are >100Å away from CD4 (Supplement 2D). The same is true if the CD3 heterodimers are positioned on opposite sides of the TCR (Supplement 2E). This is important because such estimated distances between CD4 and CD3γ or CD3ζ place them at or beyond the outer limits of detection by FRET with these probes (34, 47). That our $CD3\gamma T^{G}$::$CD4T^{mCh}$ and $CD3\zeta T^{G}$::$CD4T^{mCh}$ FRET are dependent upon the CD4 D1 domain suggests that the V-like arch identified in the crystal structures might be an initial, but not the final, arrangement of the macro-complex.

Such a conclusion is consistent with multiple studies that suggest CD4 makes contacts with class II MHC beyond those observed in the crystal structures, and may even contact the TCR-CD3 complex. For example, mutagenesis of class II MHC or the D1 and D2 domains of CD4 suggest more extensive CD4-MHC interactions than revealed by the existing structures (48–50). Furthermore, domain swap and mutagenesis analysis of the membrane proximal D3 and D4 domains of CD4 suggest additional contacts with the TCR-CD3 complex (51, 52).

In consideration of these data, it has been proposed that CD4 might pre-associate with the TCR or dock loosely along a composite surface formed by the TCR-CD3 complex to form more avid interactions than the 200μM–2mM affinity estimates for CD4 binding to MHC in isolation (1, 45). While pre-association is not supported by our data, or by super resolution imaging, such interactions could occur at a low frequency (43). Docking of CD4 along the composite surface created by TCR-CD3-pMHC would be consistent with the data presented here, and could help explain the evolutionary advantage of having weak CD4-MHC interactions in the absence of the TCR-CD3 complex. For example, CD4 binding to MHC via the D1 domain could provide sufficient interactions to facilitate preliminary nucleation of CD4 and TCR, yet be weak enough to allow for CD4 to pivot towards a more avid interaction along the TCR-CD3 composite interface. In this way, CD4 binding would be coordinated with TCR affinity, consistent with a kinetic discrimination model for TCR signaling (53). It could also help explain CD4's Lck-independent function by providing a

structural contribution to TCR-pMHC interactions that facilitates signaling (54). Also of note, interactions between the SH2 domain of Lck and phosphorylated ITAMs would not contribute to the close association observed here since the clasp domain of CD4 that interacts with Lck was replaced by a FRET probe (7, 40). But such interactions could normally extend a continuous contact interface of a compact macro-complex inside the cell that would be relevant for a recently proposed “Lck come and stay/signal duration” model (40). Additional work is needed on this long-standing problem, but the data presented here are suggestive of a compact TCR-CD3-pMHC-CD4 macro-complex that is consistent with the existing mutagenesis data.

Regardless of how CD4 and the TCR-CD3 complex achieve a close spatial relationship upon binding pMHC, the data presented here provide evidence for models in which CD4 brings Lck in closer proximity to the CD3 heterodimers than CD3ζζ. Indeed, the data indicate that the cytosolic JM regions of CD4 most closely approach the CD3δε ITAMs, suggesting that CD4-associated Lck and these ITAMs are likely to reside in the highest local concentrations upon TCR and CD4 binding of agonist pMHC. Given that experimental evidence places the cytosolic JM regions of the two CD3ε subunits within ~40Å upon assembly into the TCR-CD3 complex, and unobstructed from each other (17), the data suggest that CD4 will also bring Lck proximal to the ITAMs of the CD3γε heterodimer, particularly if the kinase domain can reach beyond its immediate locale when extended in an open and active conformation. How Lck could access the CD3ζζ ITAMs is less obvious, particularly within the context of the V-like arch stabilized by ~200μM–2mM interactions. However, if CD4 does dock along a composite TCR-CD3-pMHC surface, then interactions between CD4-associated Lck and the CD3ζζ ITAMs are more conceivable given that each CD3ζ subunit has long intracellular domains with three ITAMs that might somehow reach towards Lck. Such a docking model would also be consistent with how CD8 has been proposed to function (55, 56).

In closing, the canonical docking of TCR on class II pMHC is thought to be functionally mandated to achieve a specific relationship between Lck and the ITAMs for positive selection and T-cell activation (1, 2, 12, 13). A variety of data have predicted that CD4-associated Lck and the ITAMs of the CD3 heterodimers are most closely associated upon coordinate CD4 and TCR binding to pMHC, but this prediction has not been experimentally tested (16–19). The data herein provide evidence for a highly ordered, compact TCR-CD3-pMHC-CD4 macro-complex in which the cytosolic JM regions of CD4 are most closely associated with the JM regions of the CD3 heterodimers, and in particular the CD3δε subunits. While it would be technically challenging to temporally resolve the consequences of this apposition by ITAM phosphorylation analysis, these data provide a conceptual framework from which to devise experiments aimed at testing if the CD3δε and CD3γε ITAMs represent the ignition point for signaling under low pMHC density conditions that initiate immunological synapse formation and signal potentiation.

Supplementary Material

Refer to Web version on PubMed Central for supplementary material.

Acknowledgments

M.S.K is a Pew Scholar in the Biomedical Sciences, supported by The Pew Charitable Trusts. This work was also supported by The University of Arizona College of Medicine (M.S.K.), the Bio5 Institute (M.S.K.), and NIH/NIAID R01AI101053 (M.S.K.).

We thank Mark S. Lee and David I. Duron for thoughtful discussions, critical feedback, and technical assistance, and Dominik Schenten for critically reading the manuscript. We also thank members of the Kuhns, Nikolich-Zugich, Frelinger, Wu, and Schenten labs for critical feedback. Hemant B. Badgandi contributed novel constructs. The UACC/ALR Cytometry Core Facility and the Cancer Center Support Grant (CCSG-CA 023074) supported our flow cytometry.

References

1. Kuhns MS, Badgandi HB. Piecing together the family portrait of TCR-CD3 complexes. Immunological Reviews. 2012; 250
2. Kuhns MS, Davis MM. TCR Signaling Emerges from the Sum of Many Parts. Front Immunol. 2012; 3:159. [PubMed: 22737151]
3. Lee MS, Glassman CR, Deshpande NR, Badgandi HB, Parrish HL, Uttamapinant C, Stawski PS, Ting AY, Kuhns MS. A Mechanical Switch Couples T Cell Receptor Triggering to the Cytoplasmic Juxtamembrane Regions of CD3zetazeta. Immunity. 2015; 43:227–239. [PubMed: 26231119]
4. Minguet S, Swamy M, Alarcon B, Luescher IF, Schamel WW. Full activation of the T cell receptor requires both clustering and conformational changes at CD3. Immunity. 2007; 26:43–54. [PubMed: 17188005]
5. Gil D, Schamel WW, Montoya M, Sanchez-Madrid F, Alarcon B. Recruitment of Nck by CD3 epsilon reveals a ligand-induced conformational change essential for T cell receptor signaling and synapse formation. Cell. 2002; 109:901–912. [PubMed: 12110186]
6. Guy CS, Vignali DA. Organization of proximal signal initiation at the TCR:CD3 complex. Immunological Reviews. 2009; 232:7–21. [PubMed: 19909352]
7. Chakraborty AK, Weiss A. Insights into the initiation of TCR signaling. Nat Immunol. 2014; 15:798–807. [PubMed: 25137454]
8. Holst J, Wang H, Eder KD, Workman CJ, Boyd KL, Baquet Z, Singh H, Forbes K, Chruscinski A, Smeyne R, van Oers NS, Utz PJ, Vignali DA. Scalable signaling mediated by T cell antigen receptor-CD3 ITAMs ensures effective negative selection and prevents autoimmunity. Nat Immunol. 2008; 9:658–666. [PubMed: 18469818]
9. Guy CS, Vignali KM, Temirov J, Bettini ML, Overacre AE, Smeltzer M, Zhang H, Huppa JB, Tsai YH, Lobry C, Xie J, Dempsey PJ, Crawford HC, Aifantis I, Davis MM, Vignali DA. Distinct TCR signaling pathways drive proliferation and cytokine production in T cells. Nat Immunol. 2013; 14:262–270. [PubMed: 23377202]
10. Yoon ST, Dianzani U, Bottomly K, Janeway CA Jr. Both high and low avidity antibodies to the T cell receptor can have agonist or antagonist activity. Immunity. 1994; 1:563–569. [PubMed: 7600285]
11. Adams JJ, Narayanan S, Liu B, Birnbaum ME, Kruse AC, Bowerman NA, Chen W, Levin AM, Connolly JM, Zhu C, Kranz DM, Garcia KC. T cell receptor signaling is limited by docking geometry to peptide-major histocompatibility complex. Immunity. 2011; 35:681–693. [PubMed: 22101157]
12. Rangarajan S, Mariuzza RA. T cell receptor bias for MHC: co-evolution or co-receptors? Cell Mol Life Sci. 2014; 71:3059–3068. [PubMed: 24633202]
13. Garcia KC. Reconciling views on T cell receptor germline bias for MHC. Trends Immunol. 2012; 33:429–436. [PubMed: 22771140]
14. Wang JH, Meijers R, Xiong Y, Liu JH, Sakihama T, Zhang R, Joachimiak A, Reinherz EL. Crystal structure of the human CD4 N-terminal two-domain fragment complexed to a class II MHC molecule. Proc Natl Acad Sci U S A. 2001; 98:10799–10804. [PubMed: 11535811]

15. Yin Y, Wang XX, Mariuzza RA. Crystal structure of a complete ternary complex of T-cell receptor, peptide-MHC, and CD4. Proceedings of the National Academy of Sciences of the United States of America. 2012; 109:5405–5410. [PubMed: 22431638]
16. Kuhns MS, Davis MM. Disruption of extracellular interactions impairs T cell receptor-CD3 complex stability and signaling. Immunity. 2007; 26:357–369. [PubMed: 17368054]
17. Kuhns MS, Girvin AT, Klein LO, Chen R, Jensen KD, Newell EW, Huppa JB, Lillemeier BF, Huse M, Chien YH, Garcia KC, Davis MM. Evidence for a functional sidedness to the alphabetaTCR. Proc Natl Acad Sci U S A. 2010; 107:5094–5099. [PubMed: 20202921]
18. Fernandes RA, Shore DA, Vuong MT, Yu C, Zhu X, Pereira-Lopes S, Brouwer H, Fennelly JA, Jessup CM, Evans EJ, Wilson IA, Davis SJ. T cell receptors are structures capable of initiating signaling in the absence of large conformational rearrangements. The Journal of biological chemistry. 2012; 287:13324–13335. [PubMed: 22262845]
19. He Y, Rangarajan S, Kerzic M, Luo M, Chen Y, Wang Q, Yin Y, Workman CJ, Vignali KM, Vignali DA, Mariuzza RA, Orban J. Identification of the Docking Site for CD3 on the T Cell Receptor beta Chain by Solution NMR. J Biol Chem. 2015; 290:19796–19805. [PubMed: 26109064]
20. Birnbaum ME, Berry R, Hsiao YS, Chen Z, Shingu-Vazquez MA, Yu X, Waghray D, Fischer S, McCluskey J, Rossjohn J, Walz T, Garcia KC. Molecular architecture of the alphabeta T cell receptor-CD3 complex. Proc Natl Acad Sci U S A. 2014; 111:17576–17581. [PubMed: 25422432]
21. Call ME, Pyrdol J, Wiedmann M, Wucherpfennig KW. The organizing principle in the formation of the T cell receptor-CD3 complex. Cell. 2002; 111:967–979. [PubMed: 12507424]
22. Sun ZY, Kim ST, Kim IC, Fahmy A, Reinherz EL, Wagner G. Solution structure of the CD3epsilondelta ectodomain and comparison with CD3epsilongamma as a basis for modeling T cell receptor topology and signaling. Proc Natl Acad Sci U S A. 2004; 101:16867–16872. [PubMed: 15557001]
23. Call ME, Wucherpfennig KW, Chou JJ. The structural basis for intramembrane assembly of an activating immunoreceptor complex. Nature immunology. 2010; 11:1023–1029. [PubMed: 20890284]
24. Kim KJ, Kanellopoulos-Langevin C, Merwin RM, Sachs DH, Asofsky R. Establishment and characterization of BALB/c lymphoma lines with B cell properties. J Immunol. 1979; 122:549–554. [PubMed: 310843]
25. Letourneur F, Malissen B. Derivation of a T cell hybridoma variant deprived of functional T cell receptor alpha and beta chain transcripts reveals a nonfunctional alpha-mRNA of BW5147 origin. Eur J Immunol. 1989; 19:2269–2274. [PubMed: 2558022]
26. Parrish HL, Glassman CR, Keenen MM, Deshpande NR, Bronnimann MP, Kuhns MS. A Transmembrane Domain GGxxG Motif in CD4 Contributes to Its Lck-Independent Function but Does Not Mediate CD4 Dimerization. PLoS One. 2015; 10:e0132333. [PubMed: 26147390]
27. Hedrick SM, Matis LA, Hecht TT, Samelson LE, Longo DL, Heber-Katz E, Schwartz RH. The fine specificity of antigen and Ia determinant recognition by T cell hybridoma clones specific for pigeon cytochrome c. Cell. 1982; 30:141–152. [PubMed: 6181895]
28. Newell EW, Ely LK, Kruse AC, Reay PA, Rodriguez SN, Lin AE, Kuhns MS, Garcia KC, Davis MM. Structural basis of specificity and cross-reactivity in T cell receptors specific for cytochrome c-I-E(k). J Immunol. 2011; 186:5823–5832. [PubMed: 21490152]
29. Parrish HL, Deshpande NR, Vasic J, Kuhns MS. Functional evidence for TCR-intrinsic specificity for MHCII. Proc Natl Acad Sci U S A. 2016
30. Mayer ML. Crystal structures of the GluR5 and GluR6 ligand binding cores: molecular mechanisms underlying kainate receptor selectivity. Neuron. 2005; 45:539–552. [PubMed: 15721240]
31. Mayer ML, Olson R, Gouaux E. Mechanisms for ligand binding to GluR0 ion channels: crystal structures of the glutamate and serine complexes and a closed apo state. J Mol Biol. 2001; 311:815–836. [PubMed: 11518533]
32. Armstrong N, Gouaux E. Mechanisms for activation and antagonism of an AMPA-sensitive glutamate receptor: crystal structures of the GluR2 ligand binding core. Neuron. 2000; 28:165–181. [PubMed: 11086992]

33. Reddy Chichili VP, Kumar V, Sivaraman J. Linkers in the structural biology of protein-protein interactions. Protein Sci. 2013; 22:153–167. [PubMed: 23225024]
34. Zal T, Gascoigne NR. Using live FRET imaging to reveal early protein-protein interactions during T cell activation. Curr Opin Immunol. 2004; 16:418–427. [PubMed: 15245734]
35. Antczak AJ, Tsubota T, Kaufman PD, Berger JM. Structure of the yeast histone H3-ASF1 interaction: implications for chaperone mechanism, species-specific interactions, and epigenetics. BMC Struct Biol. 2006; 6:26. [PubMed: 17166288]
36. Brant DA, Miller WG, Flory PJ. Conformational Energy Estimates for Statistically Coiling Polypeptide Chains. J Mol Biol. 1967; 23:47-&.
37. Amet N, Lee HF, Shen WC. Insertion of the designed helical linker led to increased expression of tf-based fusion proteins. Pharm Res. 2009; 26:523–528. [PubMed: 19002568]
38. Beemiller P, Jacobelli J, Krummel MF. Integration of the movement of signaling microclusters with cellular motility in immunological synapses. Nat Immunol. 2012; 13:787–795. [PubMed: 22751140]
39. Huse M, Klein LO, Girvin AT, Faraj JM, Li QJ, Kuhns MS, Davis MM. Spatial and temporal dynamics of T cell receptor signaling with a photoactivatable agonist. Immunity. 2007; 27:76–88. [PubMed: 17629516]
40. Stepanek O, Prabhakar AS, Osswald C, King CG, Bulek A, Naeher D, Beaufils-Hugot M, Abanto ML, Galati V, Hausmann B, Lang R, Cole DK, Huseby ES, Sewell AK, Chakraborty AK, Palmer E. Coreceptor scanning by the T cell receptor provides a mechanism for T cell tolerance. Cell. 2014; 159:333–345. [PubMed: 25284152]
41. Schrum AG, Gil D, Dopfer EP, Wiest DL, Turka LA, Schamel WW, Palmer E. High-sensitivity detection and quantitative analysis of native protein-protein interactions and multiprotein complexes by flow cytometry. Sci STKE. 2007; 2007:pl2. [PubMed: 17551170]
42. Kuhns MS, Badgandi HB. Piecing together the family portrait of TCR-CD3 complexes. Immunol Rev. 2012; 250:120–143. [PubMed: 23046126]
43. Roh KH, Lillemeier BF, Wang F, Davis MM. The coreceptor CD4 is expressed in distinct nanoclusters and does not colocalize with T-cell receptor and active protein tyrosine kinase p56lck. Proc Natl Acad Sci U S A. 2015; 112:E1604–E1613. [PubMed: 25829544]
44. Minami Y, Weissman AM, Samelson LE, Klausner RD. Building a multichain receptor: synthesis, degradation, and assembly of the T-cell antigen receptor. Proceedings of the National Academy of Sciences of the United States of America. 1987; 84:2688–2692. [PubMed: 3495001]
45. Krogsgaard M, Li QJ, Sumen C, Huppa JB, Huse M, Davis MM. Agonist/endogenous peptide-MHC heterodimers drive T cell activation and sensitivity. Nature. 2005; 434:238–243. [PubMed: 15724150]
46. Brazin KN, Mallis RJ, Das DK, Feng Y, Hwang W, Wang J-h, Wagner G, Lang MJ, Reinherz EL. Structural features of the αβTCR mechanotransduction apparatus that promote pMHC discrimination. Frontiers in Immunology. 2015; 6
47. Akrap N, Seidel T, Barisas BG. Forster distances for fluorescence resonant energy transfer between mCherry and other visible fluorescent proteins. Anal Biochem. 2010; 402:105–106. [PubMed: 20347671]
48. Konig R, Huang LY, Germain RN. MHC class II interaction with CD4 mediated by a region analogous to the MHC class I binding site for CD8. Nature. 1992; 356:796–798. [PubMed: 1574118]
49. Konig R, Shen X, Germain RN. Involvement of both major histocompatibility complex class II alpha and beta chains in CD4 function indicates a role for ordered oligomerization in T cell activation. J Exp Med. 1995; 182:779–787. [PubMed: 7650484]
50. Xu H, Littman DR. A kinase-independent function of Lck in potentiating antigen-specific T cell activation. Cell. 1993; 74:633–643. [PubMed: 8358792]
51. Vignali DA, Carson RT, Chang B, Mittler RS, Strominger JL. The two membrane proximal domains of CD4 interact with the T cell receptor. J Exp Med. 1996; 183:2097–2107. [PubMed: 8642320]

52. Vignali DA, Vignali KM. Profound enhancement of T cell activation mediated by the interaction between the TCR and the D3 domain of CD4. J Immunol. 1999; 162:1431–1439. [PubMed: 9973399]

53. McKeithan TW. Kinetic proofreading in T-cell receptor signal transduction. Proc Natl Acad Sci U S A. 1995; 92:5042–5046. [PubMed: 7761445]

54. Killeen N, Littman DR. Helper T-cell development in the absence of CD4-p56lck association. Nature. 1993; 364:729–732. [PubMed: 8355789]

55. Mallaun M, Naeher D, Daniels MA, Yachi PP, Hausmann B, Luescher IF, Gascoigne NR, Palmer E. The T cell receptor's alpha-chain connecting peptide motif promotes close approximation of the CD8 coreceptor allowing efficient signal initiation. J Immunol. 2008; 180:8211–8221. [PubMed: 18523287]

56. Doucey MA, Goffin L, Naeher D, Michielin O, Baumgartner P, Guillaume P, Palmer E, Luescher IF. CD3 delta establishes a functional link between the T cell receptor and CD8. J Biol Chem. 2003; 278:3257–3264. [PubMed: 12215456]

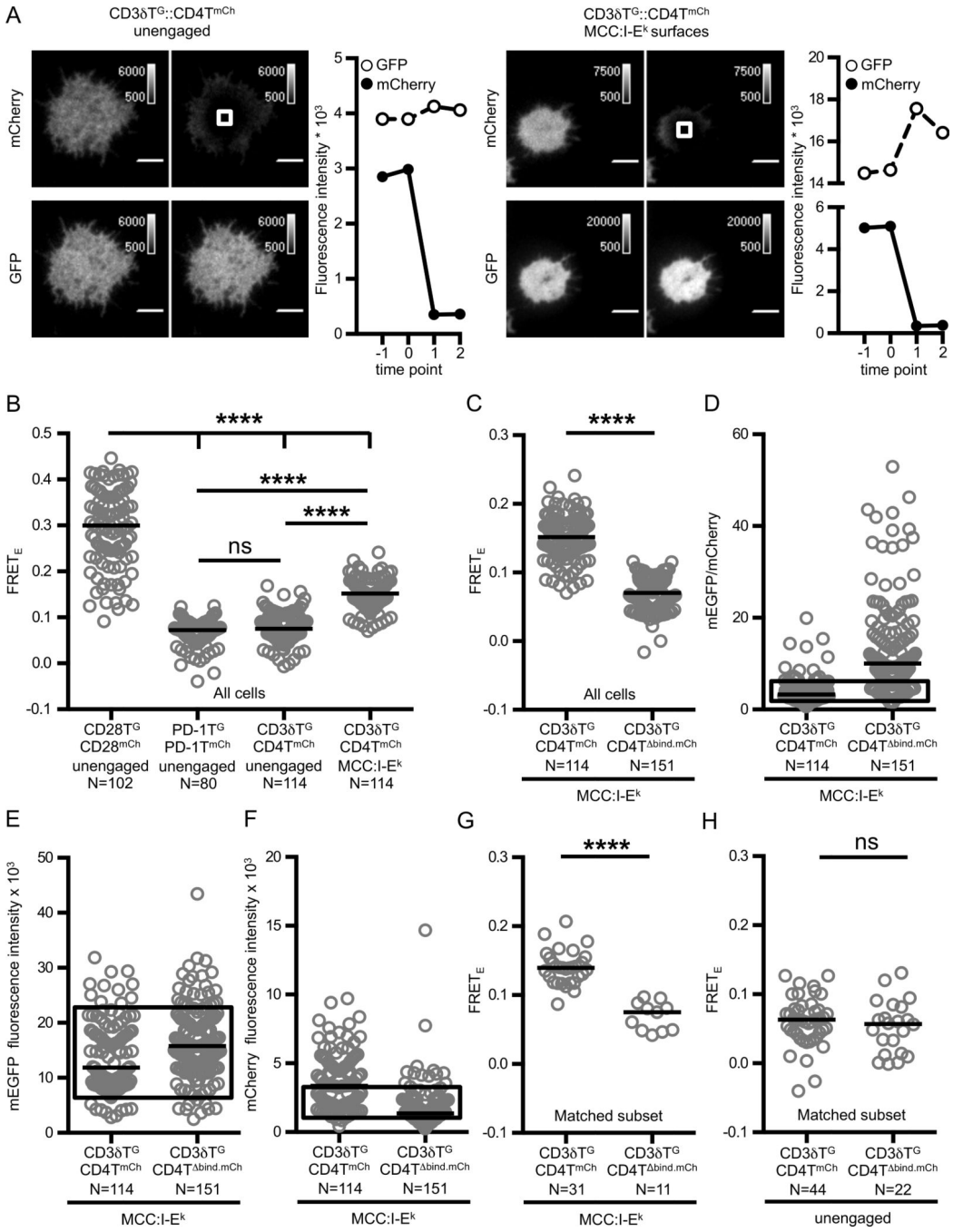

Figure 1. FRET between CD4 and CD3δ is dependent on concurrent TCR and CD4 engagement of pMHC on immobile surfaces

(A) Representative TIRF images and intensity traces showing donor recovery after acceptor photobleaching. Experimental M12 cells expressing the 5c.c7 TCR, truncated CD3 subunits and the fluorescently tagged proteins are shown adhered to glass coverslips (left: unengaged) or coverslips functionalized with MCC:I-E^k (right: TCR+CD4 engagement) as labeled and described in the text. The white box represents the region targeted for photoablation and analysis. 5μm scale bar is shown.

(B) pMHC engagement increases $FRET_E$ between CD4 and CD3δ at a population level. $FRET_E$ measurements of experimental M12 cells were compared for cells on glass coverslips (unengaged) or MCC:I-E^k functionalized coverslips as labeled and described in the text (****p<0.0001; Kruskal-Wallis with Dunn's multiple comparisons post test).
(**C**) $FRET_E$ between CD3δ and CD4 is dependent on CD4 D1 domain interactions with MHC. $FRET_E$ was measured for the indicated cell lines adhered to MCC:I-E^k functionalized coverslips as labeled (****p<0.0001; Mann-Whitney).
(**D–G**) The reduced $FRET_E$ seen with $CD4T^{\Delta bind}$ is not due to decreased accumulation of CD4 at the contact interface. Boxed region represents matched subsets from **C** for (**D**) mEGFP/mCherry ratio, (**E**) mEGFP intensity and (**F**) mCherry intensity. (**G**) Analysis of $FRET_E$ for matched subsets as shown in **D–F** and described in methods (****p<0.0001; Mann-Whitney). (**H**) The decreased $FRET_E$ observed with $CD4T^{\Delta bind}$ is dependent on MHC engagement (ns p>0.05; Mann-Whitney).
Experiments were performed and analyzed as described in Materials and Methods. Images were acquired at 500ms intervals with a 25ms exposure, 50 camera intensification. Circles represent individual cells, N= number of cells analyzed, and black bars represent median values. Data are representative of at least two experiments.

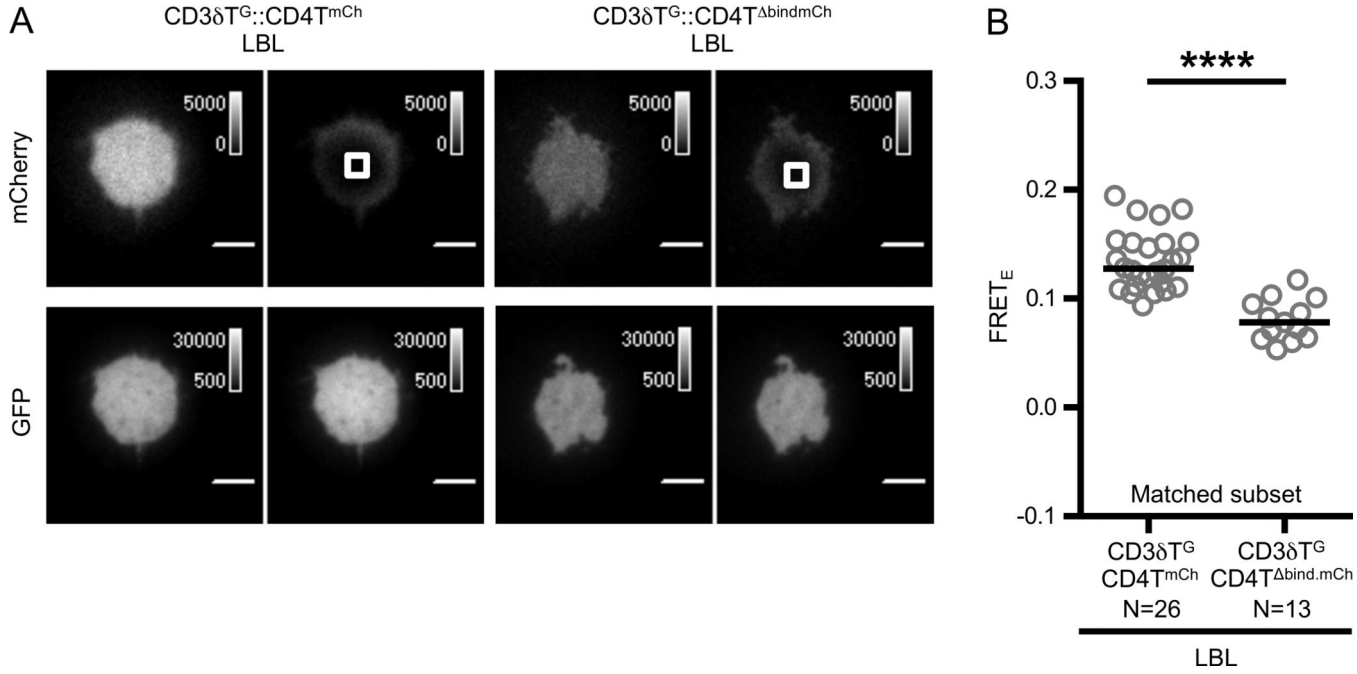

Figure 2. FRET between CD4 and CD3δ is dependent on concurrent TCR and CD4 engagement of pMHC on lipid bilayers

(A) Representative images showing donor recovery after acceptor photobleaching of experimental M12 cells adhered to supported lipid bilayers presenting MCC:I-E^k and ICAM-1 (LBL) as labeled and described in the text. Images are as described in Figure 1.

(B) CD4 D1 domain interactions with MHC are critical for observed FRET. Population analysis of matched subsets as described in Materials and Methods. Circles represent individual cells, N= number of cells analyzed, and black bars represent median values. Data are representative of at least two experiments (****$p<0.0001$; Mann-Whitney).

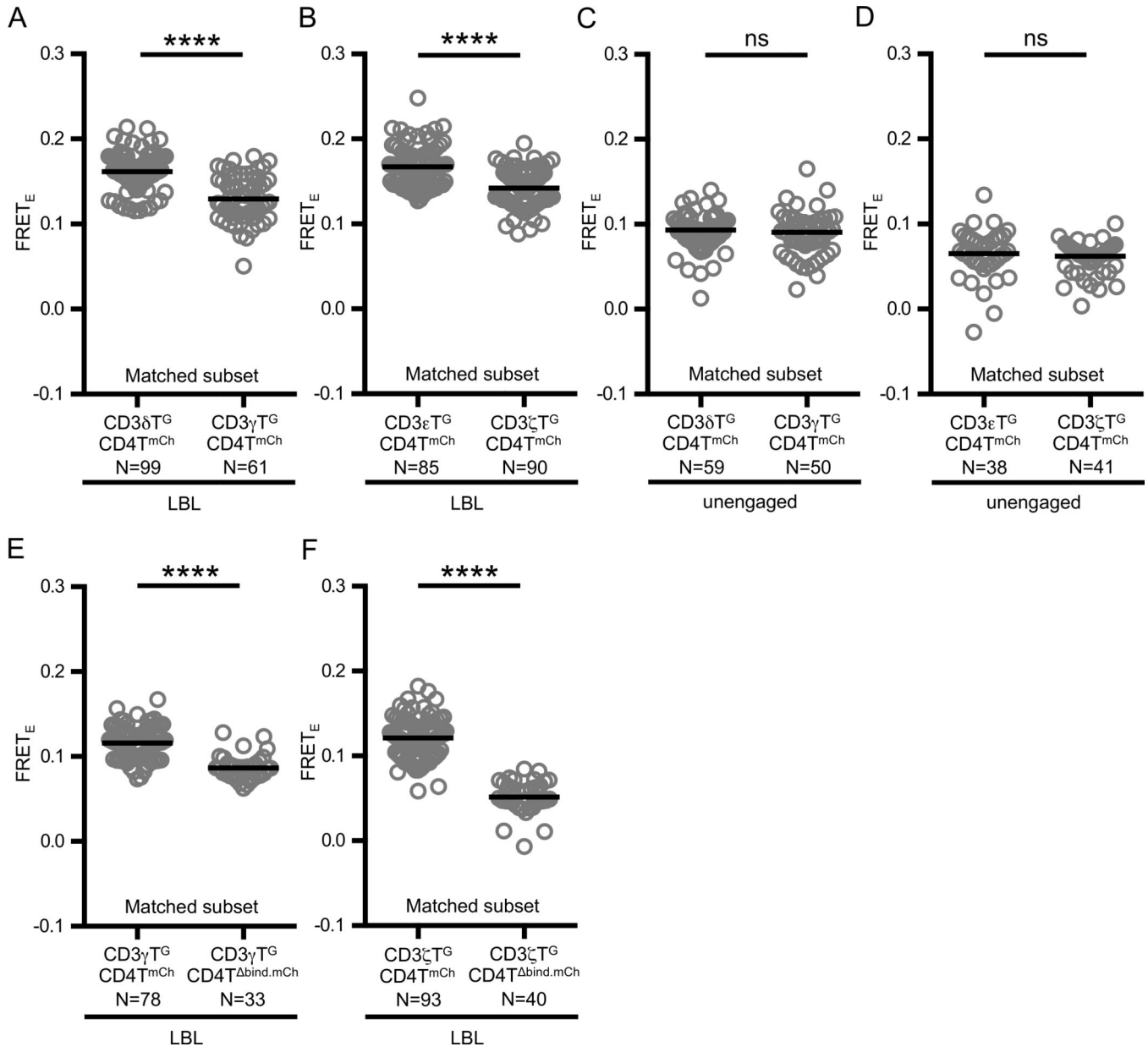

Figure 3. CD4 adopts an ordered arrangement with respect to the CD3 subunits

(A–B) Agonist pMHC engagement results in differential $FRET_E$ between CD4 and the CD3 subunits. Experimental M12 cells were adhered to supported lipid bilayers presenting MCC:I-E^k and ICAM-I (LBL) as labeled and described in the text.

(C–D) Differences in $FRET_E$ depend on ligand engagement. Experimental M12 cells were adhered to glass coverslips (unengaged).

(**E–F**) FRET between CD4 and (**E**) CD3γ or (**F**) CD3ζ subunits is dependent on CD4 D1 domain-MHC interactions. Experimental M12 cells were adhered to supported lipid bilayers presenting MCC:I-E^k and ICAM-I (LBL) as labeled and described in the text.

Circles represent individual cells, N= number of cells analyzed, and black bars represent median values. Data are representative of at least two experiments per condition. Subset

analysis and subset criteria are as detailed in Materials and Methods (****p<0.0001; Mann-Whitney).

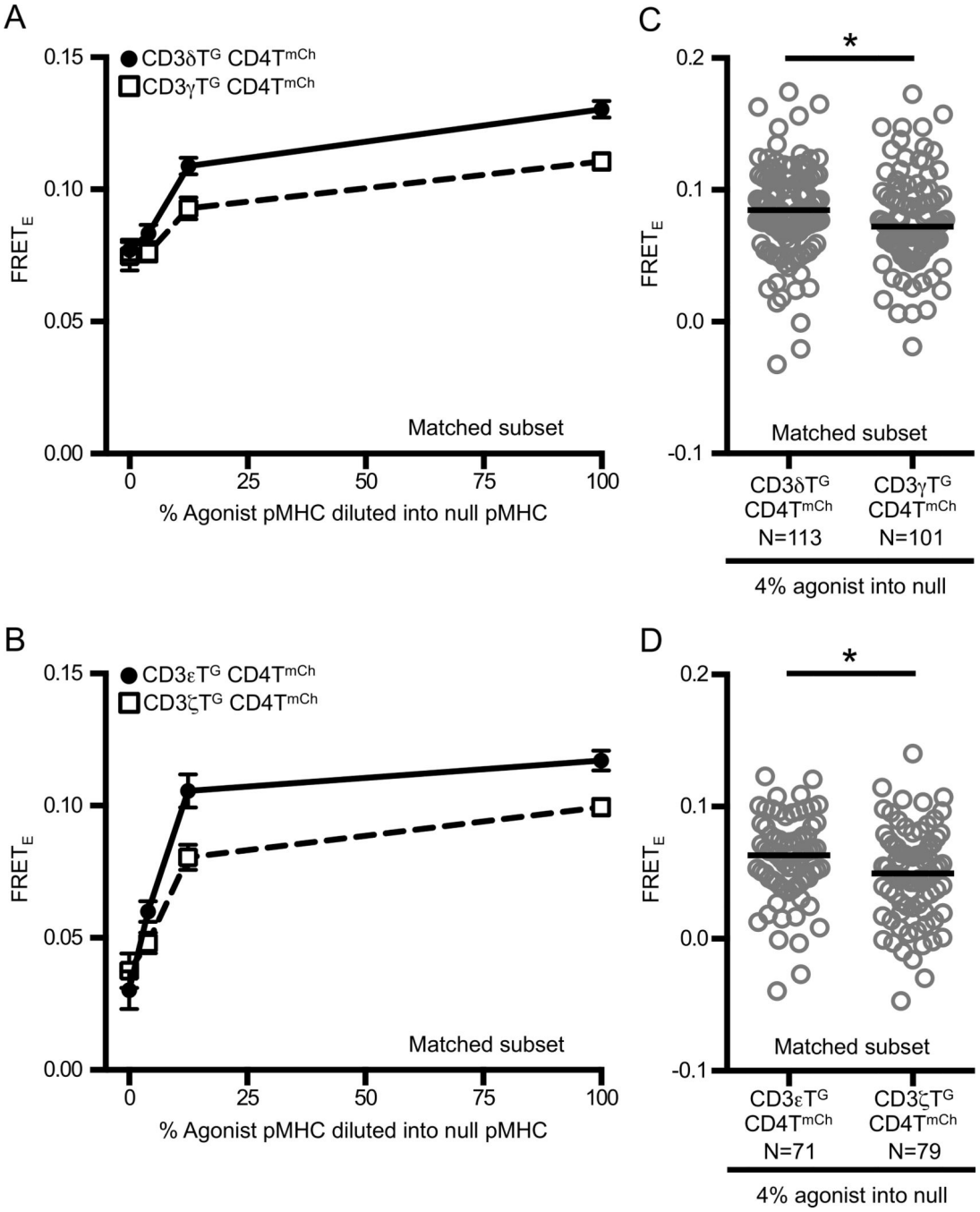

Figure 4. FRET between CD4 and CD3 subunits depends on agonist pMHC concentration

Experimental M12 cells were adhered to functionalized coverslips presenting agonist (MCC:I-E^k) diluted into null (HB:I-E^K) pMHC as labeled. The total amount of pMHC on the surface was constant. $FRET_E$ was measured and analysis was performed as described in Materials and Methods.

(A–B) Dose dependent FRET between CD4 and the CD3 subunits persists over a range of agonist pMHC concentrations. CD3δT^G::$CD4T^{mCh}$ and CD3γT^G::$CD4T^{mCh}$ did not differ on completely null surfaces [N(δ)=69, N(γ)=40, ns $p>0.05$] but did for all other ligand

concentrations tested [4% N(δ)=113, N(γ)=101, * p<0.05; 12.5% N(δ)=96, N(γ)=75, ** p<0.01; 100% N(δ)=86, N(γ)=56, ****p<0.0001]. Similarly, $CD3\varepsilon T^{G}$::$CD4T^{mCh}$ and $CD3\zeta T^{G}$::$CD4T^{mCh}$ did not differ on completely null surfaces [N(ε)=44, N(ζ)=54, ns p>0.05] but did for all other ligand concentrations tested [4% N(ε)=71, N(ζ)=79, * p<0.05; 12.5% N(ε)=52, N(ζ)=86, ** p<0.01; 100% N(ε)=55, N(ζ)=66, *** p<0.001]. Cells were intensity and ratio matched (matched subset as described in Materials and Methods) at each titration point and medians were compared using a Mann-Whitney test. Each data point in graph represents the mean +/− SEM.

(C–D) Differences between subunits persist at low ligand densities. Comparisons made on 4% agonist surfaces for matched subsets as described in Materials and Methods. Circles represent individual cells, N= number of cells analyzed, and black bars represent median values. Data are representative of at least two experiments (* p<0.05; Mann-Whitney).

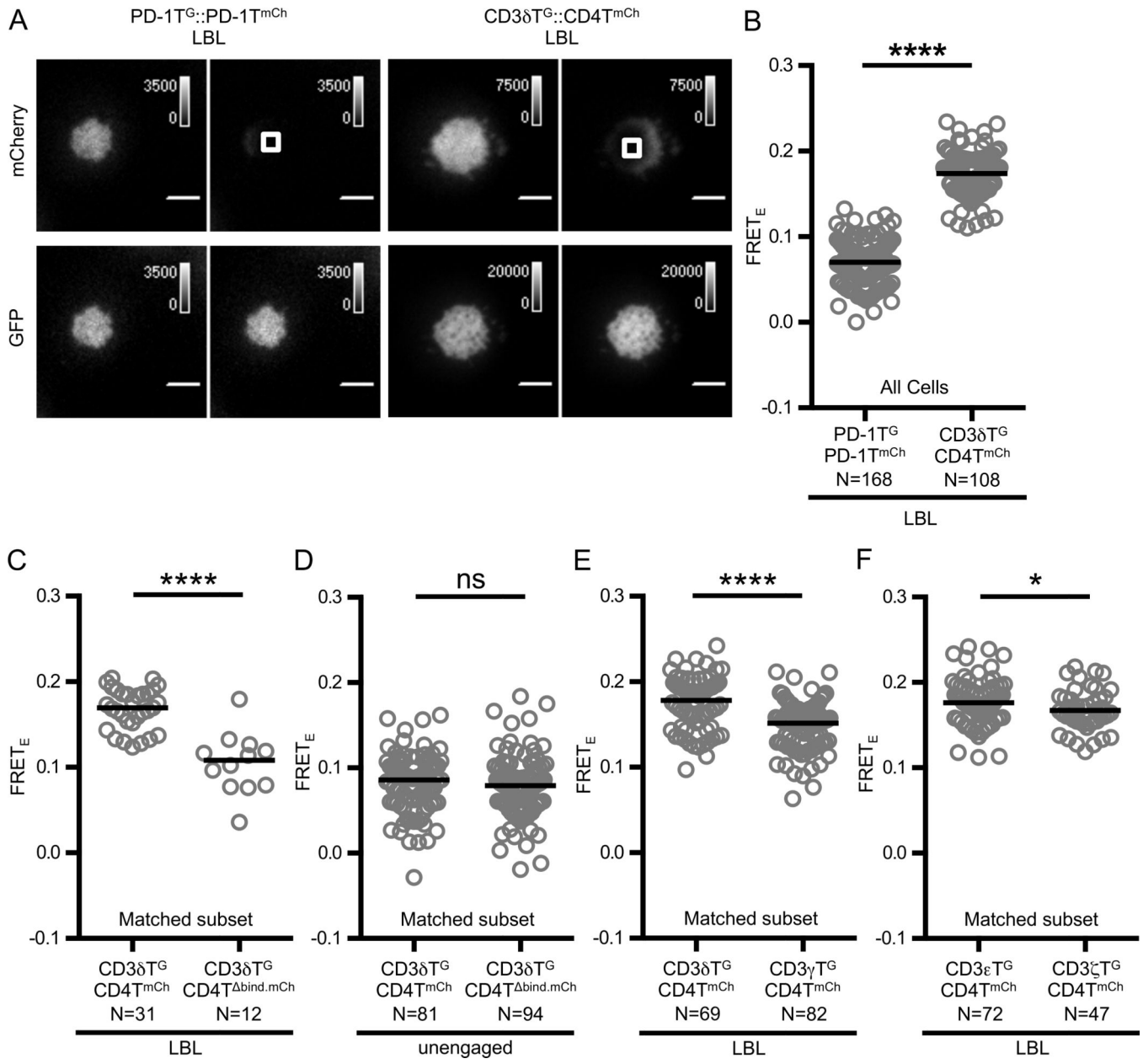

Figure 5. CD3 subunit-dependent FRET differences are maintained in 58α⁻β⁻ T-cell hybridomas

(A) Representative TIRF images of donor recovery after acceptor photobleaching for PD-1T^{G}:: PD-1T^{mCh} (left) and CD3δT^{G}::CD4^{mCh} (right) 58α^{-}β^{-} T-cell hybridomas adhered to supported lipid bilayers (LBL) presenting MCC:I-E^{k} and ICAM-1 as described in the text. Images were acquired as described in Figure 1 and Materials and Methods.

(**B**) CD3δT^{G}::CD4T^{mCh} FRET$_{E}$ is greater than PD-1T^{G}:: PD-1T^{mCh} FRET$_{E}$ on MCC-ICAM lipid bilayers in the presence of full-length CD3 subunits.

(C) FRET between CD4T and CD3δT depends on the CD4 D1 domain interacting with class II MHC.

(D) The CD4T$^{\Delta bind}$ mutation does not affect FRET efficiency in unengaged cells.

(E–F) CD4 specifically interacts with the TCR-CD3 complex in a T-cell membrane.

$FRET_E$ measurements were performed and analyzed as described in Materials and Methods. Circles represent individual cells, N= number of cells analyzed, and black bars represent median values. Data are representative of at least two experiments (* $p<0.05$, **** $p<0.0001$; Mann-Whitney).